FINITE ELEMENT CORROBORATION OF BUCKLING PHENOMENA OBSERVED IN CORRUGATED BOXES[1]

Thomas J. Urbanik

Research Engineer
USDA Forest Service
Forest Products Laboratory
One Gifford Pinchot Drive
Madison, WI 53726

and

Edmond P. Saliklis

Assistant Professor
Department of Civil and Environmental Engineering
Lafayette College
Easton, PA 18042

(Received February 2002)

ABSTRACT

Conventional compression strength formulas for corrugated fiberboard boxes are limited to geometry and material that produce an elastic postbuckling failure. Inelastic postbuckling can occur in squatty boxes and trays, but a mechanistic rationale for unifying observed strength data is lacking. This study combines a finite element model with a parametric design of the geometry and material characteristics affecting the critical buckling stress of box panels to examine their postbuckling response. The finite element model enables a broad scope of simulated panels to be examined economically. Results lead to a postbuckling model fit to the predictions and a better understanding of how to unify elastic and inelastic failure data from actual experiments and form a more general box strength formula.

Keywords: FEA, postbuckling, box compression strength, paperboard, plates.

INTRODUCTION

In accordance with the research objectives of the Agenda 2020 program of the American Forest & Paper Association, cost-saving computer-based models of corrugated fiberboard and fiberboard boxes are needed to differentiate among alternative fiber furnishes, enhance innovation in design, reduce costly destructive testing, and provide confirmation of acceptable performance. Knowing more about the fundamentals of compression strength attributes will lead to higher product performance, which can either reduce the amount of material needed to obtain necessary performance or allow unique design features so that corrugated fiberboard can compete more favorably with other materials.

Conventional box strength formulas (Batelka and Smith 1993; Hutten and Brodeur 1995; McKee et al. 1963; Shick and Chari 1965) do not relate universally to all box sizes, styles, fabrication, and materials, or to interior components. The assumed failure is by elastic buckling wherein box panels can sustain compression loads at an average failure stress σ_f greater than that predicted by the elastic critical stress σ_{cr} when bifurcation first occurs. The difference between the load carrying capacity and this theoretical strength decreases as box dimensions, relative to the combined board thickness, decrease. If box panels dis-

[1]The Forest Products Laboratory is maintained in cooperation with the University of Wisconsin. This article was written and prepared by U.S. Government employees on official time, and it is therefore in the public domain and not subject to copyright.

play a sinusoidal waviness prior to the maximum attainable load, box dimensions would generally satisfy the condition $\sigma_{cr} \leq \sigma_f \leq \sigma_y$, called elastic buckling.

The relationship among σ_{cr}, σ_f, and σ_y has been traditionally applied (Bulson 1969; Gerand 1957) to metals, with σ_y being the yield stress in compression. The same relationship prevails if expressed in terms of load per width of loading edge instead of stress. This enabled the ultimate edge crush strength P_u to be substituted for yield strength in applying the same relationship to corrugated boxes (McKee et al. 1963). Likewise, containerboard ultimate stress σ_u was successfully used in analyzing corrugated fiberboard (Urbanik 1990, 1996a). Yield stress and ultimate stress were used interchangeably in the further analysis of boxes (Urbanik 1996b, 1997). The success with using ultimate stress or ultimate strength for paper and corrugated fiberboard is fortuitous in that a yield stress for such nonlinear materials has not been defined.

Box inserts, partitions, trays, and squatty boxes can fail by an inelastic buckling phenomenon such that $\sigma_f \leq \sigma_y \leq \sigma_{cr}$. Few box compression tests to characterize strength in this regime have been reported in the literature. However, a review of some historical data bases on box compression (Urbanik 1996b), including subsets of elastic and inelastic buckling, revealed that a combination of elastic and inelastic postbuckling theory (Bulson 1969) can be universally applied to the data, with different constants for each data base, provided that nonlinear material characterization is introduced and that an empirical correction is applied to panel stiffness.

OBJECTIVE AND SCOPE

The objective of this study is to determine if the postbuckling formula advocated in Urbanik (1996b) for combined elastic and inelastic failure is supported by a parametric variation of the variables determining σ_{cr}. In the previous study (Urbanik 1996b), the best model of box strength was obtained with each panel characterized by the following two-part formula:

$$\frac{\sigma_f}{\sigma_y} = \alpha\left(\frac{\sigma_{cr}}{\sigma_y}\right)^{\eta} \qquad U > 1$$

$$\frac{\sigma_f}{\sigma_y} = \alpha \qquad U \leq 1 \tag{1}$$

together with the empirical correction

$$S_a = S\phi^{\tau} \tag{2}$$

using an apparent stiffness S_a instead of S in the calculation of σ_{cr}. Two postbuckling constants, α and η, appear in Eq. (1). A third material postbuckling constant θ_0 and a fourth constant τ are embedded implicitly in the calculation of σ_{cr} (from $\sigma_{cr} = c_1\hat{\sigma}$, per Appendix).

For nonlinear material theory, one input to σ_{cr} is the stress–strain law $\sigma = c_1 \tanh(c_2\varepsilon/c_1)$. Few reported experiments provide complete data on c_1 and c_2. In applying a nonlinear stress-strain law to the analysis of data with partial inputs, it has been found helpful to consider a constant $\theta_0 = c_1/\sigma_u$ and compute c_1 from the experimental σ_u and an optimum θ_0 representing all the data (Urbanik 1990). The optimum values of α and η via Eq. (1) then become a function of θ_0, which in turn is a function of the accuracy in determining σ_u.

Thorough experimental replication (Urbanik 1996b) and inclusion of all geometry and material variables would be prohibitively expensive. Therefore, our approach is a parametric study of the fundamental variables input to σ_{cr} combined with finite element analysis (FEA) predictions of σ_f and the application of Eqs. (1) and (2). While it makes some sense to terminate the analysis with the FEA predictions, having a simpler, yet mechanistic, strength formula can provide the basis for actual experimental confirmation and practitioner use.

The scope of our parametric design is limited to σ_{cr} as a function of the basic input variables θ_0, S, ϕ, ν, and $\hat{c}$ that comprise the theory (Johnson and Urbanik 1987) applied to simply supported plates subjected to axial compression. Other edge conditions, loading

conditions, materials, and geometry undoubtedly play a role, but their investigation is reserved until the relevancy of nonlinear material plate theory can be corroborated.

An accurate formula for σ_{cr} was reported as most important in the development of a general box compression formula (McKee et al. 1963). Variables that affect σ_y can be important but are not investigated here. In addition, just as testing procedures are known to affect an experimental σ_f, the magnitude of imperfections and the solution step size are two examples of parameters that affect the FEA prediction of σ_f.

An additional limitation to the scope of FEA is to consider only isotropic material behavior. This enables an exact characterization of the material stress–strain curve in the principal and transverse directions to be used and rules out stress–strain approximations as a source of error.

PARAMETRIC DESIGN

The theory of finite length plates (Urbanik 1996b), representing box panels and used to determine σ_{cr}, has five fundamental nondimensional inputs: θ_0, S, ϕ, ν, and $\hat{c}$. A 2^5 factorial design of these variables was generated (Table 1), with low and high values of each variable selected to include the overall scope of box panel characterization from data of four studies investigated in Urbanik (1996b) along with an inelastic regime. The curve of $\hat{\sigma}(\hat{\varepsilon})$, computed from S, ϕ, ν, and $\hat{c}$ (Fig. 1), provides a measure of the factorial range. Below $\hat{\sigma} = 0.5$, the curve is nearly linear, and plates represented by the leftmost points (Fig. 1) would likely fail by elastic buckling. Above $\hat{\sigma} = 0.9$, the represented plates would likely fail by inelastic buckling.

Isotropic plate properties h, c_2, and σ_u are given in Table 2. These properties were determined from the anisotropic inputs P_u, $E_x h$, $E_y h$, $\overline{EI}_x$, and $\overline{EI}_y$ representing the standard 205-g/m^2 C-flute corrugated fiberboard in Urbanik (2001), with the result that the computed S and ϕ of a plate would remain the same for both isotropic and anisotropic cases. Additional physical properties, c_1, ν_1, ν_2, G, d, and l, were determined from our nondimensional inputs (Table 1). Collectively, the properties shown in Tables 1 and 2 provide the material and geometry inputs for FEA characterization.

Buckling strength predictions of σ_f from the FEA model and the best fitting postbuckling formula (discussed later) are given in Table 1. The FEA predictions are simulations of edgewise compression experiments. Obviously, an exact fit to the FEA σ_f-values (Table 1) could be obtained from a 32-parameter factorial formula. With fewer-parameter formulas, parameters θ_0 and S were found to be the most significant. Thus, intermediate parametric designs with a broader range of θ_0 and S values were generated in Table 3 and additional FEA predictions were made.

FINITE ELEMENT PROCEDURE

The buckling data used to calibrate the postbuckling formula were generated by means of the commercially available finite element program ANSYS. The FEA can provide two types of buckling analyses, linear elastic classic eigenbuckling or a nonlinear analysis that tracks the response until collapse. The latter will be referred to as postbuckling analysis. Finite element postbuckling analysis can take into account material nonlinearities and initial geometric imperfections. It is a fully nonlinear static analysis with gradually increasing loads, which seeks the load level at which the structure becomes unstable.

The nonlinear buckling analysis in the FEA differs from traditional static analyses by searching for the point where the structure reaches its limit or maximum load. This is done by constantly incrementing the applied loads until the solution begins to diverge. Upon finding a final load that prevents equilibrium equations from being satisfied, the program bisects the final load step increment and attempts a new solution at a smaller load. In a buckling analysis, each such convergence failure is typically accompanied by a ‘‘nega-

TABLE 1. *Factorial design of nondimensional parameters and selected results.*

Factorial design					Physical properties						Selected results					
θ_0	S	ϕ	ν	$\hat{c}$	c_1[a] (MPa)	ν_1	ν_2[b]	G[c] (MPa)	d[d] (mm)	l[e] (mm)	FEA σ_f (Mpa)	Eq. (2) S_a	σ_{cr} (Mpa)	U	Eq. (6)[f] σ_f (Mpa)	σ_f diff. (%)
8	***0.1***	***0.25***	***0.5***	**1.25**[g]	10.9	0.5	0.5	255	32.4	130	1.26	0.05	10.6	0.36	1.20	−4.53
8	0.1	0.25	0.5	0.75	10.9	0.5	0.5	85	32.4	130	1.23[h]	0.05	10.0	0.37	1.20	−2.71
8	0.1	2	0.5	1.25	10.9	0.5	0.5	255	259	130	1.11	0.14	7.78	0.42	1.18	6.31
8	0.1	0.25	0	1.25	10.9	0	0	319	32.4	130	1.23	0.05	7.95	0.41	1.19	−3.54
8	0.1	0.25	0	0.75	10.9	0	0	191	32.4	130	1.23	0.05	7.52	0.43	1.18	−3.57
8	0.1	2	0.5	0.75	10.9	0.5	0.5	85	259	130	1.07	0.14	6.05	0.47	1.17	9.85
8	0.1	2	0	1.25	10.9	0	0	319	259	130	1.06	0.14	5.83	0.48	1.17	9.69
8	0.1	2	0	0.75	10.9	0	0	191	259	130	1.06	0.14	4.54	0.55	1.15	8.46
1	0.1	0.25	0.5	1.25	1.36	0.5	0.5	255	91.6	366	0.77	0.05	1.32	1.01	0.85	9.39
1	0.1	0.25	0.5	0.75	1.36	0.5	0.5	85	91.6	366	0.76	0.05	1.25	1.04	0.83	9.70
1	0.1	2	0.5	1.25	1.36	0.5	0.5	255	733	366	0.65	0.14	0.97	1.18	0.77	17.8
1	0.1	0.25	0	1.25	1.36	0	0	319	91.6	366	0.72	0.05	0.99	1.17	0.77	7.11
1	0.1	0.25	0	0.75	1.36	0	0	191	91.6	366	0.72	0.05	0.94	1.20	0.76	5.90
1	0.1	2	0.5	0.75	1.36	0.5	0.5	85	733	366	0.63	0.14	0.76	1.34	0.71	12.6
1	0.1	2	0	1.25	1.36	0	0	319	733	366	0.59	0.14	0.73	1.37	0.70	17.7
1	***0.1***	***2***	***0***	***0.75***	1.36	0	0	191	733	366	0.59[i]	0.14	0.57	1.55	0.64	9.86
8	***0.8***	***0.25***	***0.5***	***1.25***	10.9	0.5	0.5	255	11.4	45.8	1.31	0.38	84.8	0.13	1.33	1.76
8	0.8	0.25	0.5	0.75	10.9	0.5	0.5	85	11.4	45.8	1.42	0.38	80.2	0.13	1.33	−6.44
8	0.8	2	0.5	1.25	10.9	0.5	0.5	255	91.6	45.8	1.27	1.16	62.2	0.15	1.31	3.56
8	0.8	0.25	0	1.25	10.9	0	0	319	11.4	45.8	1.35	0.38	63.6	0.15	1.31	−2.64
8	0.8	0.25	0	0.75	10.9	0	0	191	11.4	45.8	1.41	0.38	60.1	0.15	1.31	−7.29
8	0.8	2	0.5	0.75	10.9	0.5	0.5	85	91.6	45.8	1.25	1.16	48.4	0.17	1.30	3.86
8	0.8	2	0	1.25	10.9	0	0	319	91.6	45.8	1.26	1.16	46.7	0.17	1.29	2.51
8	0.8	2	0	0.75	10.9	0	0	191	91.6	45.8	1.26	1.16	36.3	0.19	1.28	1.42
1	0.8	0.25	0.5	1.25	1.36	0.5	0.5	255	32.4	130	1.24	0.38	10.6	0.36	1.20	−3.00
1	0.8	0.25	0.5	0.75	1.36	0.5	0.5	85	32.4	130	1.23	0.38	10.0	0.37	1.20	−2.27
1	0.8	2	0.5	1.25	1.36	0.5	0.5	255	259	130	1.04	1.16	7.78	0.42	1.18	13.6
1	0.8	0.25	0	1.25	1.36	0	0	319	32.4	130	1.22	0.38	7.95	0.41	1.19	−2.91
1	0.8	0.25	0	0.75	1.36	0	0	191	32.4	130	1.22	0.38	7.52	0.43	1.18	−3.00
1	0.8	2	0.5	0.75	1.36	0.5	0.5	85	259	130	1.01	1.16	6.05	0.47	1.17	15.5
1	0.8	2	0	1.25	1.36	0	0	319	259	130	1.02	1.16	5.83	0.48	1.17	14.9
1	***0.8***	**2**	***0***	***0.75***	1.36	0	0	191	259	130	1.30[j]	1.16	4.54	0.55	1.15	−11.5

[a] $c_1 = \sigma_u\theta_0$.
[b] $\nu_1 = \nu_2 = \nu$.
[c] $G = [(\hat{c} - \nu)/2(1 - \nu^2)]c_2$.
[d] $d = \phi l$.
[e] $l = \sqrt{12EI/\theta_0 SP_u}$.
[f] Parameter values from Model 7 in Table 4.
[g] Design in bold italics is also in Table 3.
[h] Run 10.
[i] Run 5.
[j] Run 7.

tive pivot,'' which means that the attempted load equals or exceeds the buckling load. The program normally converges to the limiting load as the process of bisection and resolution continues to the point at which the minimum load increment is achieved. The minimum load step will directly affect the precision of results. For this study, the FEA inputs that prescribe how iteration shall seek out this final buckling load were kept constant. Depending on the geometry and material properties, the final collapse state of stress may be less or greater than the classical eigenbuckling stress.

Our finite element postbuckling analyses used 8-noded isoparametric shell elements. Twelve elements per buckled shape (sinusoi-

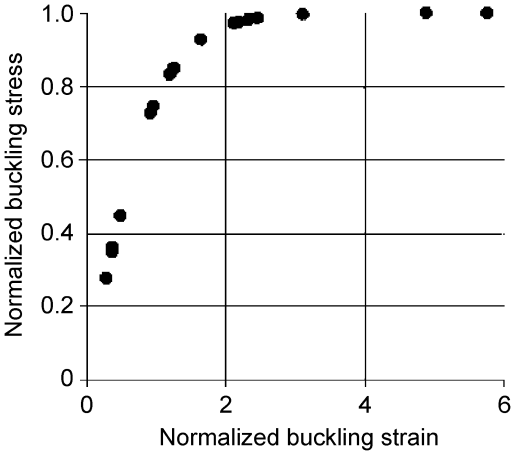

FIG. 1. Variation of normalized buckling stress $\hat{\sigma}$ (Eq. (A-13)) with normalized buckling strain $\hat{\varepsilon}$ (Eq. (A-2)) for inputs from factorial design in Table 1 and nonlinear stress–strain law.

dal half-wave) were used in typical mesh sizes (Fig. 2). This mesh size was chosen based on mesh refinement exercises. Isotropic material characterization enabled input of the exact stress–strain curve, $\sigma = c_1 \tanh(c_2\varepsilon/c_1)$. The Poisson's ratio varied from 0 to 0.49. At $\nu = 0$, the shear modulus G is one-half the modulus of elasticity E. At $\nu = 0.5$, the material is incompressible.

Another feature of nonlinear buckling analysis is that if the loading on the structure is perfectly in-plane (membrane or axial stresses only), the out-of-plane deflections necessary to initiate buckling will not develop and the analysis will fail to predict buckling behavior. To initiate some out-of-plane movement resulting from in-plane compressive loads, a small out-of-plane perturbation, such as a modest temporary force or a prescribed displacement, must be applied. The final failure load is very sensitive to these parameters. Consequently, we kept the initial imperfection consistent with the longest dimension of the panel to simulate nearly perfect, yet real, panels. For panels up to 100 mm long, the initial imperfection was 1 mm out-of-plane, bowing from the edges to the center of the panel. For 100- to 500-mm panels, the imperfection was 2 mm. For panels longer than 500 mm on either edge, the imperfection was 3 mm.

TABLE 2. *Isotropic properties of standard corrugated fiberboard.*

Property	Value
P_u	8.150 kN/m
$\overline{EI} = \sqrt{\overline{EI}_x\overline{EI}_y}$	9.117 Nm
$Eh = \sqrt{E_x h E_y h}$	3,054 kN/m
$h = \sqrt{12\overline{EI}/Eh}$	5.985 mm
$E = Eh/h$	510.3 MPa
$c_2 = E$	510.3 MPa
$\sigma_u = P_u/h$	1.362 MPa

To more realistically simulate experimental laboratory results, the postbuckling analysis imposed a downward displacement at the top of the panel, which simulated the head movement of a testing machine. The bottom of the panel was not allowed to translate vertically. All edges were pinned (i.e., allowed to rotate) and remained straight (i.e., did not displace transverse to the panel). As the top of the panel was forced downward, the panel bulged outward into a number of half-sine waves. Stresses increased throughout the analysis, until convergence could no longer be achieved. Maximum out-of-plane displacement was recorded throughout the analysis, as was the final number of half-sine waves. The total force along the loaded edge was recorded throughout the analysis. Typical results for applied and out-of-plane displacement are shown for run 5 ($\sigma_f \geq \sigma_{cr}$) and run 10 ($\sigma_f \leq \sigma_{cr}$) in Fig. 3. For run 5, the maximum average stress was approximately 586 kPa, as reported in Table 1, even though the panel had not yet collapsed. Final collapse occurred shortly afterwards, at 520 kPa.

RESULTS

The FEA determinations of σ_f are summarized in Table 1 for the factorial designs and in Table 3 for the intermediate designs. Various forms of Eq. (1) using either a linear material law or a nonlinear law to compute σ_{cr} were fit to the data. Note that the second line

TABLE 3. *Intermediate designs of nondimensional parameters and selected results.*

Intermediate design					Physical properties						Selected results					
											FEA	Eq. (2)			Eq. (6)[f]	
θ_0	S	ϕ	ν	$\hat{c}$	c_1[a] (MPa)	ν_1	ν_2[b]	G[c] (MPa)	d[d] (mm)	l[e] (mm)	σ_f (MPa)	S_a	σ_{cr} (MPa)	U	σ_f (MPa)	σ_f diff. (%)
1	0.145	2	0	0.75	1.36	0	0	191	609	304	0.76	0.210	0.82	1.29	0.73	−4.91
1	0.012	2	0	0.75	1.36	0	0	191	2,094	1047	0.35	0.018	0.07	4.43	0.33	−5.97
1	0.008	2	0	0.75	1.36	0	0	191	2,555	1278	0.29	0.012	0.05	5.40	0.29	−0.50
1	0.004	2	0	0.75	1.36	0	0	191	3,885	1942	0.21	0.005	0.02	8.22	0.22	3.48
2	0.042	2	0	0.75	2.72	0	0	191	798	399	0.81	0.061	0.48	1.69	0.61	−24.6
2	0.020	2	0	0.75	2.72	0	0	191	1,146	573	0.49	0.030	0.23	2.42	0.48	−1.92
2	0.006	2	0	0.75	2.72	0	0	191	2,126	1063	0.35	0.009	0.07	4.49	0.32	−8.93
2	0.005	2	0	0.75	2.72	0	0	191	2,439	1219	0.26	0.007	0.05	5.16	0.29	11.6
4	0.042	0.25	0.5	1.25	5.45	0.5	0.5	255	70.6	282	0.92	0.020	2.23	0.78	1.00	8.93
4	0.020	0.25	0.5	1.25	5.45	0.5	0.5	255	101	405	0.79	0.010	1.08	1.12	0.79	0.03
4	0.006	0.25	0.5	1.25	5.45	0.5	0.5	255	188	751	0.55	0.003	0.31	2.08	0.53	−2.60
4	0.005	0.25	0.5	1.25	5.45	0.5	0.5	255	216	862	0.48	0.002	0.24	2.39	0.49	0.44
8	0.145	0.25	0.5	1.25	10.9	0.5	0.5	255	26.9	108	1.14	0.069	15.4	0.30	1.23	7.79
8	0.012	0.25	0.5	1.25	10.9	0.5	0.5	255	92.5	370	0.94	0.006	1.30	1.02	0.84	−10.2
8	0.008	0.25	0.5	1.25	10.9	0.5	0.5	255	113	452	0.82	0.004	0.87	1.25	0.74	−9.68
8	0.004	0.25	0.5	1.25	10.9	0.5	0.5	255	172	687	0.64	0.002	0.38	1.90	0.56	−11.5
1	***0.1***	***2***	***0***	***0.75***	1.36	0		191	733	366	0.59	0.145	0.57	1.55	0.64	9.86
1	0.4	2	0	0.75	1.36	0	0	191	366	183	1.07	0.579	2.27	0.77	1.01	−5.98
1	0.5	2	0	0.75	1.36	0	0	191	328	164	1.15	0.723	2.84	0.69	1.09	−5.81
1	***0.8***	***2***	***0***	***0.75***	1.36	0	0	191	259	130	1.30	1.157	4.54	0.55	1.15	−11.5
2	0.2	2	0	0.75	2.72	0	0	191	366	183	1.21	0.289	2.27	0.77	1.01	−16.9
2	0.3	2	0	0.75	2.72	0	0	191	299	150	1.27	0.434	3.40	0.63	1.14	−10.4
2	0.6	2	0	0.75	2.72	0	0	191	212	106	1.31	0.868	6.81	0.45	1.18	−10.3
2	0.7	2	0	0.75	2.72	0	0	191	196	98	1.34	0.013	7.94	0.41	1.19	−11.6
4	0.2	0.25	0.5	1.25	5.45	0.5	0.5	255	32.4	130	1.12	0.096	10.6	0.36	1.20	6.96
4	0.3	0.25	0.5	1.25	5.45	0.5	0.5	255	26.4	106	1.14	0.143	15.9	0.29	1.23	7.84
4	0.6	025	0.5	1.25	5.45	0.5	0.5	255	18.7	75	1.30	0.287	31.8	0.21	1.27	−1.97
4	0.7	0.25	0.5	1.25	5.45	0.5	0.5	255	17.3	69	1.30	0.334	37.1	0.19	1.28	−1.49
8	***0.1***	***0.25***	***0.5***	***1.25***	10.9	0.5	0.5	255	32.4	130	1.26	0.048	10.6	0.36	1.20	−4.53
8	0.4	0.25	0.5	1.25	10.9	0.5	0.5	255	16.2	65	1.30	0.191	42.4	0.18	1.29	−0.88
8	0.5	0.25	0.5	1.25	10.9	0.5	0.5	255	14.5	58	1.30	0.239	53.0	0.16	1.30	0.07
8	***0.8***	***0.25***	***0.5***	***1.25***	10.9	0.5	0.5	255	11.4	46	1.31	0.382	84.8	0.13	1.33	1.76

of Eq. (1) is the same as the first line when $\eta = 0$. An even more general form of Eq. (1) is obtained by making the substitutions $\sigma_{cr} = \sigma c_1$ and $\sigma_y = \sigma_u = c_1/\theta_0$ to get

$$\sigma_f = \alpha {\sigma_y}^{1-\eta} {\sigma_{cr}}^{\eta} = \alpha c_1 {\theta_0}^{\eta-1} \hat{\sigma}^{\eta} \tag{3}$$

and prescribing α and η as a function of U. An algorithm for determining $\hat{\sigma}$ from inputs S, ϕ, ν, and $\hat{c}$ is given in the Appendix. If S_a is then substituted for S according to Eq. (2), θ_0 becomes an additional input and it is helpful to write σ_f as

$$\sigma_f = \alpha \sigma_1 {\theta_0}^{\eta-1} {\hat{\sigma}_a}^{\eta} \tag{4}$$

to express $\hat{\sigma}$ as an apparent stress $\hat{\sigma}_a$.

Working with nondimensional $\hat{\sigma}$ instead of σ_{cr} via Eq. (3) also provides a way to investigate a linear stress–strain law. In accordance with Johnson and Urbanik's (1987) theory, implementing the linear stress–strain law puts $\hat{\sigma}$ into the form $\hat{\sigma} = CS$ (from Eq. A-3), which leads to

$$\sigma_f = \alpha c_1 {\theta_0}^{\eta-1} (CS)^{\eta} \tag{5}$$

If we then substitute S_a from Eq. (2) again, we get

$$\sigma_f = \alpha c_1 {\theta_0}^{\eta-1} (CS_a)^{\eta} \tag{6}$$

This interesting solution of buckling in terms of C while retaining c_1 and θ_0 as inputs pro-

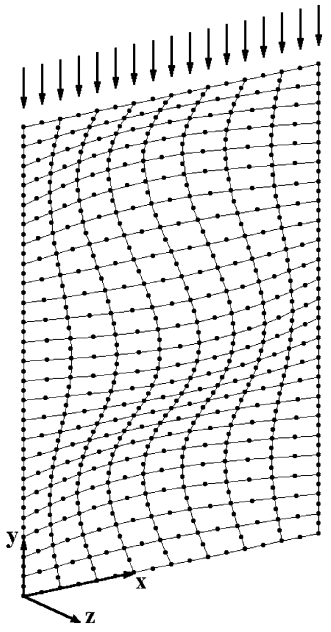

FIG. 2. Buckling plate subjected to uniform displacement along top edge with all edges simply supported and restrained from *z*-direction translation. Actual analysis used 12 elements per half-wave.

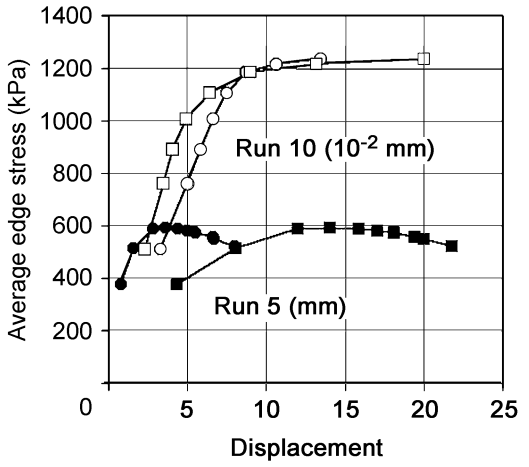

FIG. 3. Variation of out-of-plane displacement (squares) with average edge stress corresponding to applied downward displacement (circles) and determined by FEA algorithm in nonlinear buckling analysis of runs 5 and 10 in Table 1. Note two displacement scales.

duces a sort of hybrid stress–strain theory. Although the prediction of σ_f incorporates a linear material law, parameters c_1 and θ_0 appear in the formula and enable nonlinear stress–strain curves to be input. This is analogous to a tangent modulus theory where some remote slope along a nonlinear stress–strain curve gets treated as the initial modulus in a linear theory.

A summary of the models obtained from Eqs. (3) to (6) is given in Table 4. For comparison, Model 1 is simply the McKee formula from McKee et al. (1963) rearranged into Eq. (5) with constants α and η taken from Urbanik (1997). The average error magnitude and the correlation coefficient reported (Table 4) are

TABLE 4. *Parameter values of 13 models fit to FEA data.*

Law	Model	τ	$U \le U_b$		U_b[a]	$U \ge U_b$		Ave. |error| (%)	r^2	Error ratio[b]
			α_1	η_1		α_2	η_2			
McKee	1	0	—	—	—	0.394	0.254	26.2	0.638	17.1
Linear Eq. (5)	2	0	—	—	—	0.551	0.175	15.8	0.700	5.3
	3	0	0.808	0	1	0.808	0.382	16.8	0.707	4.8
	4	0	0.750	0.060	0.621	0.609	0.280	9.7	0.856	2.4
Hybrid Eq. (6)	5	0.559	—	—	—	0.555	0.202	14.9	0.754	4.1
	6	0.716	0.832	0	1	0.832	0.447	13.6	0.806	3.3
	7	0.533	0.798	0.049	0.647	0.628	0.325	7.1	0.936	1.0
Nonlinear Eq. (3)	8	0	—	—	—	0.636	0.250	15.6	0.699	4.8
	9	0	0.826	0	1	0.826	0.357	16.1	0.747	4.4
	10	0	0.737	0.119	1.000	0.737	0.349	12.3	0.810	3.1
Nonlinear Eq. (4)	11	0.410	—	—	—	0.636	0.264	14.8	0.720	4.4
	12	0.760	0.778	0	1	0.778	0.416	13.3	0.851	3.3
	13	0.620	0.809	0.073	0.922	0.766	0.407	9.4	0.883	1.8

[a] $U_b = \exp[0.5 \ln(\alpha_1/\alpha_2)/(\eta_1 - \eta_2)]$.
[b] Normalized relative to lowest sum of errors squared determined on logarithmic scale.

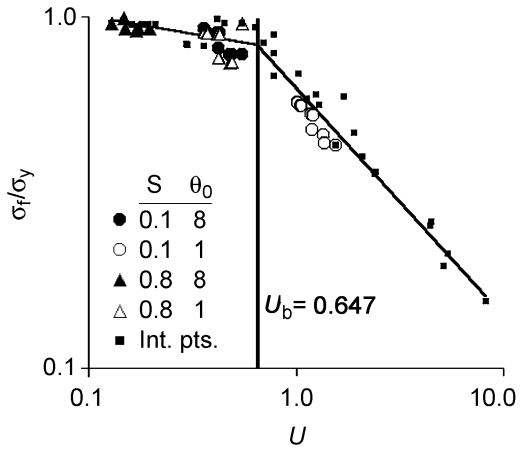

FIG. 4. Variation of stress ratio σ_f/σ_y with universal slenderness U for data in Tables 1 and 3. Bilinear line is fit of best-fitting Model 7 from Table 4. Here and in Figures 5 and 6, the data include levels of S (0.1, 0.8) and θ_0 (1, 8) along with intermediate design points (Int. pts.).

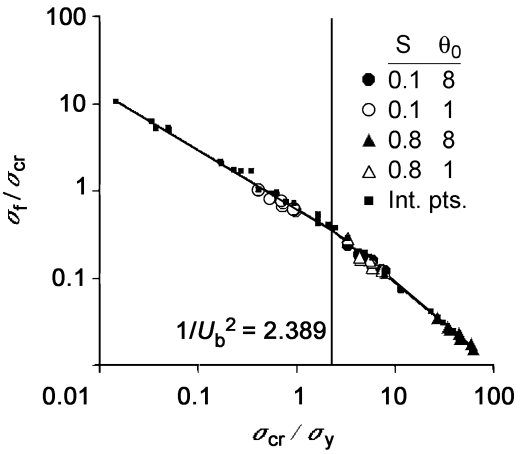

FIG. 5. Variation of stress ratio σ_f/σ_{cr} with ratio σ_{cr}/σ_y for data in Tables 1 and 3. Bilinear line is fit of best-fitting Model 7 from Table 4.

between the FEA σ_f values (Tables 1 and 3) and the postbuckling model of σ_f. Only the σ_f predictions from postbuckling Model 7 are reported in Tables 1 and 3.

Various criteria can be used to compare the fit of each postbuckling model with FEA predictions. The average error magnitude of 26.2% for Model 1 (Table 4) was reduced to 15.8% for Model 2 by optimizing the α and η values in Eq. (5) to match the FEA predictions. The differences in α and η between Model 1 and Model 2 are a measure of how our derived physical properties and the FEA characterization compare to the real box panels in actual experiments (McKee et al. 1963).

The average error magnitude was reduced as expected per our parametric design with a combined elastic–inelastic postbuckling model. This is observable in Table 4 by comparing Models 2 and 3, Models 5 and 6, Models 8 and 9, and Models 11 and12. Elastic failure occurs among the data when $U \geq U_b$, and inelastic failures occur when $U \leq U_b$, with U_b considered a breakpoint among the U data. The case when $U_b = 1$ and inelastic $\eta = 0$ is the same as Eq. (1).

The elastic–inelastic models were made more accurate by optimizing U_b and generalizing the separation between elastic and inelastic data. This is observable in Table 4 by comparing Models 3 and 4 and Models 9 and 10. For each case of elastic or elastic–inelastic model, the average error magnitude was further reduced by substituting S_a for S and determining an optimum τ, and corroborates with actual experiments (Urbanik 1996b). This is observable in Table 4 by comparing Models 5, 6, and 7 with Models 2, 3, and 4, respectively, and Models 11, 12, and 13 with Models 8, 9, and 10, respectively.

In the analysis of actual experiments (Urbanik 1996b), nonlinear material theory fit data better than did linear material theory, but with the elastic–inelastic model restricted to the form of Eq. (1). Our results of Model 9 compared with Model 3 (Table 4) are consistent. However, for our FEA data, the hybrid material law, not previously considered, appears best. This can be observed in Table 4 by comparing Models 5 and 7 with Models 11 and 13, respectively. Note that for the hybrid law to be used, the material must still be characterized as nonlinear and S_a must be substituted for S.

Figures 4, 5, and 6 are plots of the best-fitting Model 7 (Table 4) with an average error magnitude of 7.1%. Figure 4 is a representa-

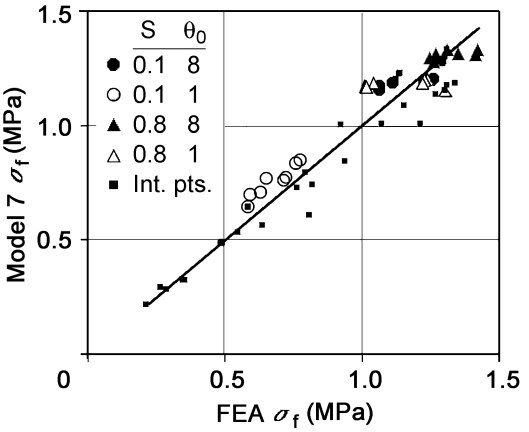

FIG. 6. Comparison of σ_f values in Tables 1 and 3 with FEA determinations.

tion of the generated data as utilized in Bulson (1969) and Urbanik (1996b). Plates represented by points with $U > U_b = 0.647$ fail by elastic buckling. Plates with $U < U_b$ fail by inelastic buckling. As mentioned previously, few experiments have addressed the important variables in inelastic failure. The transition between elastic and inelastic buckling around U_b (Fig. 4) is even less understood.

A rearrangement of Eq. (6) gives rise to the apparent stiffness given by

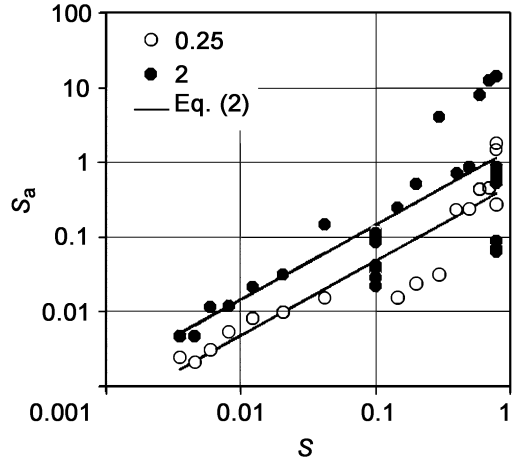

FIG. 7. Variation of apparent stiffness S_a with S. Points are determinations of S_a from Eq. (7) at two levels of ϕ. Lines are predictions according to Eq. (2).

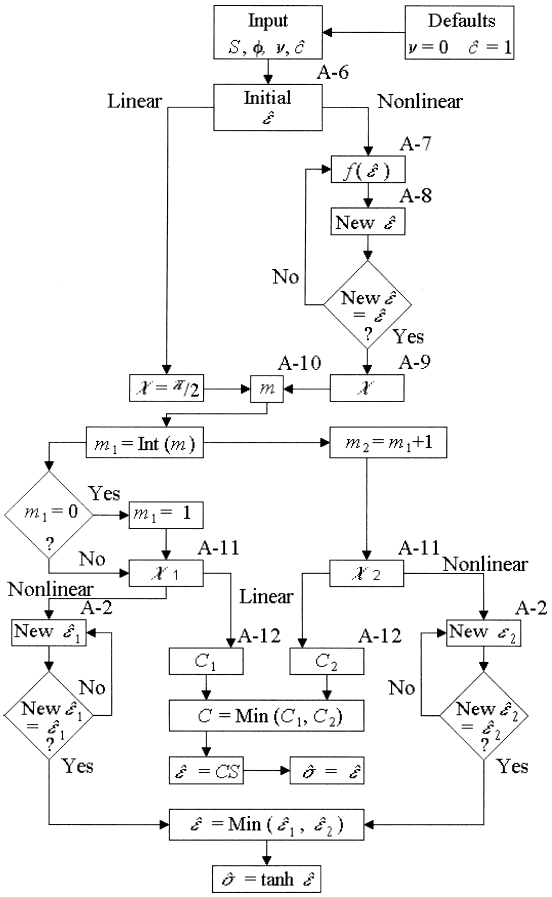

FIG. 8. Solution of $\hat{\sigma}$ from specified S, ϕ, ν, and $\hat{c}$ and a linear or a nonlinear material law. Letter–number labels (A-6, A-7, etc.) refer to equation numbers in Table 5.

$$S_a = \frac{1}{C}\left(\frac{\sigma_f \theta_0^{1-\eta}}{\alpha c_1}\right)^{1/\eta} \tag{7}$$

Figure 7 shows how predictions of S_a given by Eq. (2) compare with the exact determinations by Eq. (7), with α and η inputs from Model 7, and provides a good validation of why such a correction for an apparent stiffness succeeded with actual experiments (Urbanik 1996b).

CONCLUSIONS

The postbuckling of plates with nonlinear material and subjected to axial compression was analyzed with a finite element model. Various models were fit to the finite element predictions to determine a simplified form of a

TABLE 5. *Equations referred to by letter-number labels in Fig. 8.*

Eq.	Form	Reference
(A-2)	$\text{New } \hat{\varepsilon} = \dfrac{\dfrac{4\hat{\varepsilon}^2}{\tanh(2\hat{\varepsilon})} + \left[\dfrac{1}{1-\nu^2}\left(\hat{c} + \dfrac{\pi^2}{4\chi^2}\right)^2 - \dfrac{\hat{c}-1}{1-\nu^2} - 1\right]\sinh(2\hat{\varepsilon})}{\dfrac{4\hat{\varepsilon}}{\tanh(2\hat{\varepsilon})} + \dfrac{3}{\chi^2 S}\sinh(2\hat{\varepsilon}) - 2}$	Eq. (A-2), Appendix
(A-6)	$\hat{\varepsilon} = \dfrac{\pi^2 S(\hat{c}+1)}{6(1-\nu^2)}$	Eq. (3.5′), Urbanik (1992)
(A-7)	$f(\hat{\varepsilon}) = 1 - \dfrac{2\hat{\varepsilon}}{\sinh(2\hat{\varepsilon})}$	Johnson and Urbanik (1987)
(A-8)	$\text{New } \hat{\varepsilon} = \dfrac{\pi^2 S}{6(1-\nu^2)}\left[\hat{c} + \sqrt{1-(1-\nu^2)f(\hat{\varepsilon})}\right]$	Eq. (3.4), Urbanik (1992)
(A-9)	$\chi = \dfrac{\pi}{2}[1-(1-\nu^2)f(\hat{\varepsilon})]^{1/4}$	Eq. (3.3), Johnson and Urbanik (1987)
(A-10)	$m = \dfrac{2\chi\phi}{2\phi}$	Eq. (9), Urbanik (1996b)
(A-11)	$\chi_i = \dfrac{m_i\pi}{2\phi}$	Eq. (10), Urbanik (1996b)
(A-12)	$C = \dfrac{\chi^2}{3(1-\nu^2)}\left[\left(\hat{c} + \dfrac{\pi^2}{4\chi^2}\right)^2 - \hat{c}^2 + 1\right]$	Eq. (A-4), Appendix
(A-13)	$\hat{\sigma} = \tanh\hat{\varepsilon}$	Eq. (5.1), Johnson and Urbanik (1987)

more general strength formula applicable to the panels of corrugated containers. An empirical correction for plate stiffness as a function of an effective plate aspect ratio input to an elastic–inelastic postbuckling model with an empirically optimized division between elastic and inelastic failures gave the best results. The postbuckling model corroborates experimental data, and results extend the strength predictability of panels of boxes with geometry beyond the range available from actual experiments.

NOMENCLATURE

C Eq. (A-4)

c_1, c_2 Constants in the y-direction stress–strain relationship $\sigma = c_1 \tanh(c_2\varepsilon/c_1)$

$\hat{c}$ Normalized in-plane shear modulus of elasticity given by $\hat{c} = \nu + 2(1-\nu^2)(G/c_2)\sqrt{\nu_2/\nu_1}$. When $\hat{c} = 1$, St. Venant's principle prevails.

D_x, D_y Plate bending stiffness in x-direction and y-direction, respectively, wherein $D = \overline{EI}/(1-\nu_1\nu_2)$

d, l, h y-direction plate depth, x-direction plate width, and plate thickness, respectively

E Modulus of elasticity

E_xh, E_yh Combined board extensional stiffness per unit width perpendicular (E_xh) and parallel (E_yh) to fluting axis

$\overline{EI}_x$, $\overline{EI}_y$ Combined board bending stiffness per unit width perpendicular ($\overline{EI}_x$) and parallel ($\overline{EI}_y$) to fluting axis

$f(\hat{\varepsilon})$ Eq. (A-7)

G In-plane shear modulus of elasticity

$g(\hat{\varepsilon})$ Zero function

m Number of buckled half-waves along d

P_u Combined board edgewise compression strength

r	Coefficient of correlation
S	Normalized plate stiffness given by $S = (c_2/c_1)(h/l)^2\sqrt{\nu_1/\nu_2} = 12\sqrt{\overline{EI}_x\overline{EI}_x}/\theta_0 P_u l^2$
S_a	Empirically corrected apparent S
U	Universal plate slenderness given by $U = \sqrt{\sigma_y/\sigma_{cr}}$
U_b	U-breakpoint between elastic and inelastic postbuckling
x, y	Plate axis in transverse and loaded directions, respectively
α, η	Postbuckling constants
ε	Strain
ε_{cr}	Critical strain
$\hat{\varepsilon}$	Normalized buckling strain
θ_0	Nonlinear material postbuckling constant given by $\theta_0 = c_1/\sigma_u$
ϕ	Effective plate aspect ratio given by $\phi = (d/l)(D_x/D_y)^{1/4}$
τ	Stiffness correction exponent
ν, ν_1, ν_2	Geometric mean $\sqrt{\nu_1\nu_2}$ and Poisson's ratios associated with x- and y-direction plate loading, respectively
χ	Nondimensional wave period
σ	Stress
σ_{cr}	Average critical stress at bifurcation across plate width
σ_f	Average failure stress across plate width at maximum load
σ_u	Material ultimate stress
σ_y	Material yield stress
$\hat{\sigma}$	Normalized buckling stress

REFERENCES

Batelka, J. J., and C. N. Smith. 1993. Package compression model. Containerboard and Kraft Paper Group, Project 3746, Final Report. February. American Forest & Paper Association, Washington, DC.

Bulson, P. S. 1969. The stability of flat plates. American Elsevier Publishing Company, Inc., New York, NY.

Gerand, G. 1957. Handbook of structural stability. Part IV. Failure of plates and composite elements. Natl. Adv. Comm. for Aeronautics, Tech. Note 3874. August.

Hutten, M., and P. Brodeur. 1995. MD and CD properties of linerboard components and the resulting box stacking performance. Containerboard and Kraft Paper Group Project 3712, Final Report, July. American Forest & Paper Association, Washington, DC.

Johnson, M. W., Jr., and T. J. Urbanik. 1987. Buckling of axially loaded, long rectangular plates. Wood Fiber Sci. 19(2):135–146.

McKee, R. C., J. W. Gander, and J. R. Wachuta. 1963. Compression strength formula for corrugated boxes. Paperboard Packaging (August).

Shick, P. E., and N. C. S. Chari. 1965. Top-to-bottom compression for double wall corrugated boxes. Tappi J. 48(7):423–430.

Urbanik, T. J. 1990. Correcting for instrumentation with corrugated fiberboard edgewise crush test theory. Tappi J. 73(10):263–268.

———. 1992. Effect of in-plane shear modulus of elasticity on buckling strength of paperboard plates. Wood Fiber Sci. 24(4):381–384.

———. 1996a. Machine direction strength theory of corrugated fiberboard. J. Comp. Technol. Res. 18(2):80–88.

———. 1996b. Review of buckling mode and geometry effects on postbuckling strength of corrugated containers. Development, validation, and application of inelastic methods for structural analysis and design, Pressure Vessels and Piping, 343:85–94. American Society of Mechanical Engineers.

———. 1997. Linear and nonlinear material effects on postbuckling strength of corrugated containers. App. Mech. Div. vol. 221/MD vol. 77, Mechanics of Cellulosic, American Society of Mechanical Engineers. Pp. 93–99.

———. 2001. Effect of corrugated flute shape on fiberboard edgewise crush strength and bending stiffness. J. Pulp Paper Sci. 27(10):330–335.

APPENDIX

Nonlinear Stress–Strain Law

Previous research (Urbanik 1996b) considered the buckling strain of a finite length plate with fixed χ. An algorithm for finding the root of Eq. (3.2′) from Urbanik (1992)

$$g(\hat{\varepsilon}) = \frac{\chi^2 S}{3}\left[\frac{1}{1-\nu^2}\left(\hat{c} + \frac{\pi^2}{4\chi^2}\right)^2 - \frac{\hat{c}^2 - 1}{1-\nu^2} - f(\hat{\varepsilon})\right] - \hat{\varepsilon} = 0 \tag{A-1}$$

and based on fixed point iteration was proposed. For the current study, an algorithm for more general values χ and based on Newton's method is given by

$$\text{New } \hat{\varepsilon} = \hat{\varepsilon} - \frac{g(\hat{\varepsilon})}{\partial g(\hat{\varepsilon})/\partial\hat{\varepsilon}} \tag{A-2}$$

Linear Stress–Strain Law

In accordance with linear material analysis (Johnson and Urbanik 1987), the linear stress–strain law $\sigma = c_2\hat{\varepsilon}$ or $\hat{\sigma} = \hat{\varepsilon}$, agrees with Eq. (0.1) of Johnson and Urbanik (1987) for small strains. For a small strain $f(\hat{\varepsilon}) = 0(\hat{\varepsilon}^2)$

so that Eq. (2.13′) of Urbanik (1992), the linear buckling stress is

$$\hat{\sigma} = CS \tag{A-3}$$

where

$$C = \frac{\chi^2}{3}\left[\frac{1}{1-\nu^2}\left(\hat{c} + \frac{\hat{\beta}^2}{\chi^2}\right)^2 - \frac{\hat{c}^2 - 1}{1-\nu^2}\right] \tag{A-4}$$

For simple support $\hat{\beta} = \pi/2$ and the solution of Eq. (3.2′) of Urbanik (1992) for a value of χ that minimizes $\hat{\varepsilon}$ when plate length is infinite gives $\chi = \pi/2$. Hence, in this case

$$C = \frac{\pi^2(\hat{c} + 1)}{6(1-\nu^2)} \tag{A-5}$$

Please note that Eqs. (3.5′) and (5.3.1′) were given incorrectly in Urbanik (1992). With finite values of plate length, values of C_1 and C_2 corresponding to m_1 and m_2 need to be examined.

Algorithm

An algorithm for determining the nondimensional buckling stress of a simply supported plate with compression in the direction of its length and having either a linear or a nonlinear material characterization is given in Fig. 8. Referenced equations are given in Table 5. After computing $\hat{\sigma}$, the critical stress is $\sigma_{cr} = c_1\hat{\sigma}$.